JACS
JOURNAL OF THE AMERICAN CHEMICAL SOCIETY

Communication

pubs.acs.org/JACS

Driving Force Dependent, Photoinduced Electron Transfer at Degenerately Doped, Optically Transparent Semiconductor Nanoparticle Interfaces

Byron H. Farnum, Zachary A. Morseth, M. Kyle Brennaman, John M. Papanikolas, and Thomas J. Meyer*

Department of Chemistry, University of North Carolina, Chapel Hill, North Carolina 27599-3290, United States

Supporting Information

ABSTRACT: Photoinduced, interfacial electron injection and back electron transfer between surface-bound $[Ru^{II}(bpy)_2(4,4'\text{-}(PO_3H_2)_2\text{-}bpy)]^{2+}$ and degenerately doped In_2O_3:Sn nanoparticles, present in mesoporous thin films (nanoITO), have been studied as a function of applied external bias. Due to the metallic behavior of the nanoITO films, application of an external bias was used to vary the Fermi level in the oxide and, with it, the driving force for electron transfer ($\Delta G^{o\prime}$). By controlling the external bias, $\Delta G^{o\prime}$ was varied from 0 to −1.8 eV for electron injection and from −0.3 to −1.3 eV for back electron transfer. Analysis of the back electron-transfer data, obtained from transient absorption measurements, using Marcus−Gerischer theory gave an experimental estimate of λ = 0.56 eV for the reorganization energy of the surface-bound $Ru^{III/II}$ couple in acetonitrile with 0.1 M $LiClO_4$ electrolyte.

Heterogeneous electron-transfer reactions initiated by visible light excitation of molecular chromophores surface bound to wide band gap semiconductor nanoparticles provide the basis for dye-sensitized solar energy conversion strategies.[1−3] For n-type metal oxides such as TiO_2, SnO_2, and ZnO, electron injection occurs by electron transfer from a molecular excited state to the conduction band of the semiconductor with rate constants typically in the range of 10^{10}−10^{12} s^{-1}.[4−7] Back electron transfer between the injected electron and oxidized chromophore is typically orders of magnitude slower, 10^3−10^6 s^{-1}.[6,8−11] Injection and back electron transfer are illustrated in eqs 1 and 2 for a generic n-type metal oxide (MO_x) and a prototypical Ru^{II}-polypyridyl chromophore. The difference in time scales for eqs 1 and 2 provides a basis for transient redox separation and applications in dye-sensitized solar cells and dye-sensitized photoelectrosynthesis cells.[1−3,12−15]

$$MO_x\text{−}Ru^{2+} \xrightarrow{h\nu} MO_x\text{−}Ru^{2+*} \rightarrow MO_x(e^-)\text{−}Ru^{3+} \quad (1)$$

$$MO_x(e^-)\text{−}Ru^{3+} \rightarrow MO_x\text{−}Ru^{2+} \quad (2)$$

Electron injection into nanostructured metal oxides, monitored by ultrafast transient absorption measurements, has been shown to be adequately described by Marcus−Gerischer theory.[4,6,16,17] Within this framework, the rate constant for interfacial electron transfer, dictated by the requirement for energy conservation, is determined by the energetic overlap of electronic levels in the semiconductor with the distribution of activation energies in the reacting molecule.[16−19] Similar success has not been realized for back electron transfer where there is limited evidence for a free-energy dependence.[20−22] Efforts in this area have been complicated by slow, complex electron-transfer kinetics at the interface believed to be the result of trap-state limited electron diffusion through the metal oxide nanostructures.[6,8,9,11,23,24]

Here we report the results of an investigation on photoinduced electron injection and back electron transfer for the surface-bound chromophore, $[Ru^{II}(bpy)_2(4,4'\text{-}(PO_3H_2)_2\text{-}bpy)]^{2+}$ (RuP^{2+}: bpy is 2,2′-bipyridine, Figure S2) on mesoporous In_2O_3:Sn nanoparticle films (nanoITO) by transient absorption spectroscopy. The results are novel in taking advantage of the metallic properties of the degenerately doped transparent conductive oxide (TCO) nanoparticles to avoid complications from electron diffusion in the oxide allowing a focus on the electron-transfer characteristics of a single-site, surface-bound molecule. Further, doping densities >10^{20} cm^{-3} allow for band bending of only a few nanometers at the nanoparticle surface such that the Fermi level at the nanoITO/solution interface can be controlled through an applied external bias.[25−27] This has allowed, heretofore, unprecedented experimental access to the driving force dependence of interfacial electron transfer for a single molecular site. The results are interpreted by application of Marcus−Gerischer theory which provides a direct estimate of the reorganization energy for the single-site, surface-bound $Ru^{III/II}$ redox couple.

Thin (3 μm) films of nanoITO were deposited on SnO_2:F (FTO) coated glass by a doctor blade technique from an ITO nanoparticle (10−20 nm diameter) dispersion. The resulting films were annealed under two different conditions: (1) 500 °C/1 h in air (oxidized; nanoITO(ox)) and (2) 500 °C/1 h in air followed by 300 °C/1 h under H_2(5%)/N_2 gas flow (reduced; nanoITO(red)). UV−vis near-IR absorbance spectral comparisons between the two materials revealed a noticeable blue shift in the localized surface plasmon resonance (LSPR) in the near-IR following the second, reductive annealing step, Figure S2. This feature has been noted elsewhere and arises from an increase in electron density for the reduced oxide.[27−32] The LSPR feature could be simulated by application of the standard Drude analysis giving estimated electron densities of N = 3.1 and 7.8 × 10^{20} cm^{-3} for oxidized and reduced nanoITO, respectively, Figure S2.[32,33]

Received: August 27, 2014
Published: October 20, 2014

The band gap transition at $\lambda < 400$ nm was also found to be blue-shifted for reduced nanoITO with respect to oxidized films consistent with conduction band filling known as the Burstein–Moss effect.[34]

Oxidized and reduced nanoITO films were surface derivatized with RuP^{2+} by soaking overnight in methanol solutions with $[RuP](Cl)_2$ = 0.5 mM. Figure S1 shows UV–vis absorbance spectra of oxidized and reduced nanoITO–RuP^{2+} films recorded in acetonitrile (MeCN) with 0.1 M $LiClO_4$ electrolyte. Saturated surface coverages of $\Gamma = 3.1$ and 2.7×10^{-8} mol cm^{-2} for oxidized and reduced nanoITO, respectively, were estimated from UV–vis absorbance spectra. See Supporting Information for further details.[35]

Derivatized nanoITO–RuP^{2+} films were used as the working electrode in three-electrode spectroelectrochemical cells in order to monitor spectral changes on the ps–ns time scale by transient absorption measurements as a function of applied bias. A constant external bias, E_{app}, was applied to the nanoITO–RuP^{2+} electrode during the transient absorption experiment and varied in 0.2 V increments from 1.0 to −0.8 V vs SCE. Ohmic losses were small in the spectroelectrochemical cell, and the applied bias was assumed to define the equilibrated Fermi level (E_F) throughout the nanoITO film. The applied potential range was dictated by the reduction potentials for the metal-centered Ru^{III}/Ru^{II}, $E^{o\prime}(-RuP^{3+/2+})$ = 1.30 V vs SCE, and ligand-based $Ru^{II}(4,4'\text{-}(PO_3H_2)_2\text{-bpy})^{2+}/Ru^{II}(4,4'\text{-}(PO_3H_2)_2\text{-bpy}^{\bullet-})^{+}$), $E^{o\prime}(-RuP^{2+/+})$ = −1.53 V, couples to avoid background electrochemical reactions. Steady-state UV–vis spectra recorded before and after transient absorption measurements showed no sign of irreversible decomposition of the surface-bound chromophores.

Figure 1 illustrates representative transient absorbance difference spectra at the indicated delay times following 420 nm pulsed laser excitation (0.7 mJ cm^{-2}) of nanoITO(ox)–RuP^{2+} at E_{app} = 1.0 V. The features that appear in the transient spectra were general to both oxidized and reduced nanoITO and are consistent with loss of the characteristic, ground-state metal-to-ligand charge transfer (MLCT) absorption features in the visible due to formation of the excited state, $-RuP^{2+}*$. Appearance of the excited state was complete by 1 ps, followed by electron injection, eq 1, which occurred from 1 ps to 1 ns. Electron injection was monitored most directly by observing the change in ΔAbs signal at 375 nm where an initial positive $\pi \rightarrow \pi^*(4,4'\text{-}(PO_3H_2)_2\text{-bpy}^{\bullet-})$ absorption feature for the MLCT excited state decayed over time to yield ground-state bleach features representative of $-RuP^{3+}$ and nanoITO(e^-).[28] Back electron transfer between nanoITO(e^-) and $-RuP^{3+}$, eq 2, was observed on the ns–μs time scale during which the transient absorption features returned to the baseline with reformation of nanoITO–RuP^{2+}.

The time scale for electron injection was found to be highly dependent on the applied external bias. Figure S3 shows single wavelength ΔAbs traces at 375 nm as a function of E_{app} from 1.0 to −0.8 V for nanoITO(ox)–RuP^{2+}. As E_{app} was decreased, the time scale for $\Delta Abs_{375\ nm}$ decay increased from tens of picoseconds to hundreds of picoseconds consistent with slower electron injection. A potential dependence for injection is expected as the driving force was varied with applied bias where $\Delta G^{o\prime}_{inj} = -F(E_F - E^{o\prime}(RuP^{3+/2+}*))$, with F Faraday's constant, E_F (= E_{app}) the Fermi level in the oxide and $E^{o\prime}(RuP^{3+/2+}*)$ = −0.78 V vs SCE for the $-Ru^{III}(4,4'\text{-}(PO_3H_2)_2\text{-bpy})^{3+}/-Ru^{III}(4,4'\text{-}(PO_3H_2)_2\text{-bpy}^{\bullet-})^{2+}*$ couple. Based on the applied potentials, $\Delta G^{o\prime}_{inj}$ was calculated to vary from −1.8 to 0 eV.

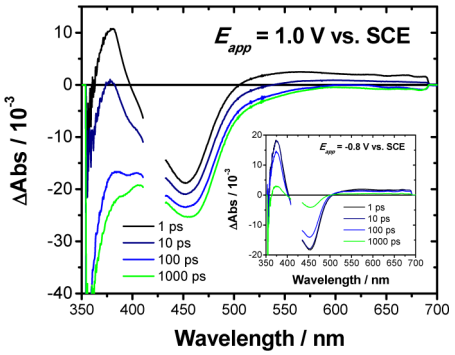

Figure 1. Transient absorbance difference spectra recorded at the indicated delay times for nanoITO(ox)–RuP^{2+} electrodes in MeCN (0.1 M $LiClO_4$) at E_{app} = 1.0 V vs SCE at room temperature. (inset) Transient absorption difference spectra recorded at E_{app} = −0.8 V for the same sample.

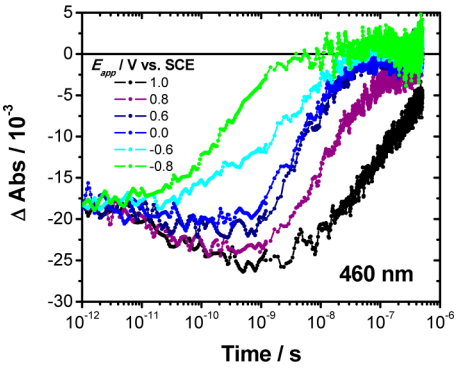

Figure 2. Single wavelength transient absorbance traces recorded at 460 nm as a function of E_{app} for nanoITO(ox)–RuP^{2+} in MeCN (0.1 M $LiClO_4$).

Beyond $E_{app} < -0.2$ V the formation of $-RuP^{3+}$ and nanoITO(e^-) was less evident in the transient spectra. At E_{app} = −0.8 V, the difference spectra were only characteristic of excited-state decay, Figure 1 inset. The kinetics for $-RuP^{2+}*$ decay under these conditions was found to be nearly first-order on both oxidized and reduced nanoITO with lifetimes of 380 and 290 ps, respectively. These values are notably decreased compared to the characteristic excited-state lifetime of 840 ns measured on the surface of the inert oxide ZrO_2 in MeCN (0.1 M $LiClO_4$) at room temperature, Figure S4. This observation points to participation by one or more additional pathways for excited state decay on nanoITO at $E_{app} < -0.2$ V. The origin of this effect is currently under investigation.

In the range E_{app} = 1.0–0 V, back electron transfer was monitored at 460 nm, Figure 2. At the most positive applied bias of 1.0 V the ΔAbs signal decreased over the first 1000 ps due to conversion from $-RuP^{2+}*$ to $-RuP^{3+}$ by electron injection. As shown in Figure 2, back electron transfer occurred on the ns–μs time scale with an obvious increase in rate as the applied bias was decreased from 1.0 to 0 V. Near E_{app} = 0 V, the rate of back electron transfer reached a bias-independent plateau. At more negative applied potentials complications appeared from incomplete electron injection and competing excited-state decay, as described above and shown in Figure 2 for E_{app} = −0.6 and −0.8 V, thus limiting analysis of the data to $E_{app} > 0$ V.

As is commonly observed at metal oxide interfaces, back electron-transfer kinetics were complex and nonexponential.[6,8,9,11] The data were analyzed as the characteristic time for

dx.doi.org/10.1021/ja508862h | J. Am. Chem. Soc. 2014, 136, 15869–15872

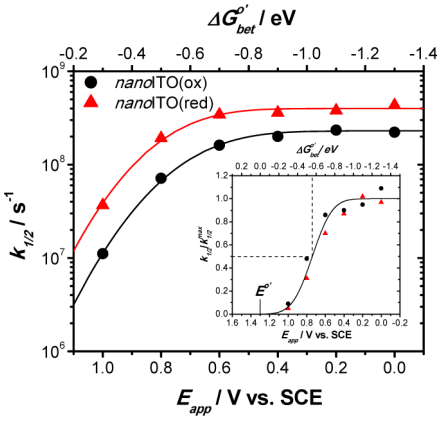

Figure 3. Back electron transfer rate constants reported as $k_{1/2}$ for $\Delta Abs_{460\ nm}$ decay as a function of E_{app} and $\Delta G^{o\prime}{}_{bet}$ for nanoITO(ox) (black circles) and nanoITO(red) (red triangles).

1/2 of the ΔAbs signal to decay to zero ($t_{1/2}$) or as the inverse rate constant, $k_{bet} = k_{1/2} = 1/t_{1/2}$.[10,20] Figure 3 shows values of $k_{1/2}$ for back electron transfer measured on oxidized and reduced nanoITO plotted versus E_{app}. These data illustrate that $k_{1/2}$ increased as E_{app} was varied from 1.0 to 0 V, reaching limiting values of $k_{1/2}{}^{max} = 2.3$ and $4.0 \times 10^8\ s^{-1}$ for oxidized and reduced nanoITO, respectively. As calculated from $\Delta G^{o\prime}{}_{bet} = -F(E^{o\prime}(RuP^{3+/2+}) - E_F)$ with $E^{o\prime}(RuP^{3+/2+}) = 1.30$ V vs SCE and $E_F = E_{app}$, the driving force for back electron transfer was varied from −0.3 to −1.3 eV.

The driving force dependence of back electron transfer was analyzed using Marcus−Gerischer theory, eq 3.[16−19] Here, $g(E)$ is the distribution of electronic levels in nanoITO as a function of energy, $f(E,E_F)$ is the Fermi function that describes the occupancy of electronic levels at energy E, $H_{ab}(E)$ is the electron-transfer coupling matrix element, and $W(E)$ is the Gaussian distribution of classical activation energies. From Marcus theory in the classical, harmonic limit, $W(E)$ is given by eq 4 where λ is the total reorganization energy, intramolecular (λ_i) plus solvent (λ_o), and $\Delta G(E)$ is the driving force for electron transfer at energy E.

$$k_{bet} = \frac{2\pi}{\hbar}\int_{-\infty}^{\infty} g(E)f(E,E_F)|H_{ab}(E)|^2 W(E)dE \quad (3)$$

$$W(E) = \frac{1}{\sqrt{4\pi\lambda kT}}\exp\left(\frac{-(\Delta G(E)+\lambda)^2}{4\lambda kT}\right) \quad (4)$$

The Marcus−Gerischer model differs from the standard Marcus approach in that electron transfer from nanoITO to $-RuP^{3+}$ occurs over the range of energy levels below the Fermi level (i.e., $E > E_F$) with each occurring isoenergetically.[17,19] Contributions from these levels are included in the overlap integral in eq 3 with the integral dominated by energies where both $g(E)$ and $W(E)$ are large. For metals, $g(E)$ is nearly constant over all E; however, for semiconductors, $g(E)$ is only large within the conduction and valence bands but is ∼0 within the band gap. Degenerately doped semiconductors such as nanoITO "bridge the gap" between metals and semiconductors by providing a large density of dopant levels within the band gap. Given the metallic behavior of nanoITO,[34,36] $g(E)$ was assumed to be constant with $g(E) \sim NV$ where N is the electron density and V is the volume of occupied electronic levels. With this assumption, eqs 3 and 4 simplify to eqs 5 and 6 for $k_{1/2}$ and $k_{1/2}{}^{max}$, respectively. In these equations $H_{ab}(E)$ is assumed to be constant, and the low temperature limit is assumed for $f(E, E_F)$. Based on eq 5, the driving force dependence of $k_{1/2}$ is governed by the integrated value of $W(E)$ for the $-RuP^{3+/2+}$ couple. This equation can be solved directly by integrating from E_F to ∞ to give eq 7 with $\Delta G^{o\prime}{}_{bet}$ defined previously.

$$k_{1/2} = k_{1/2}^{max}\int_{E_F}^{\infty}\frac{1}{\sqrt{4\pi\lambda kT}}\exp\left(\frac{-(\Delta G(E)+\lambda)^2}{4\lambda kT}\right)dE \quad (5)$$

$$k_{1/2}^{max} = \frac{2\pi}{\hbar}H_{ab}{}^2 NV \quad (6)$$

$$k_{1/2} = (k_{1/2}^{max}/2)\left[1 - \mathrm{erf}\left(\frac{\Delta G_{bet}^{o\prime} + \lambda}{2\sqrt{\lambda kT}}\right)\right] \quad (7)$$

Iterative fits of the data in Figure 3 to eq 7 with the $k_{1/2}{}^{max}$ values cited above resulted in $\lambda = 0.60$ and 0.52 eV for oxidized and reduced nanoITO, respectively, giving an average value of $\lambda = 0.56 \pm 0.04$ eV. This value for λ is close to values found for $[Ru(bpy)_3]^{3+/2+}$ self-exchange in aqueous solution with $\lambda = 0.4$[37] and 0.57[38] eV having been reported and attributed mainly to solvent reorganization (λ_o). Although not an overly sensitive probe, this result suggests that the solvent environment around the surface-bound $-RuP^{3+/2+}$ couple is comparable to fluid solution. This is in contrast to models for interfacial electron transfer that predict partial desolvation and decreases in λ_o compared to a fluid.[18,19]

A prediction of the Marcus−Gerischer model that follows from eq 7 is that at $-\Delta G^{o\prime}{}_{bet} = \lambda$, $k_{1/2} = k_{1/2}{}^{max}/2$ or $k_{bet} = k_{bet}{}^{max}/2$. This is in contrast to a reaction between discrete molecules in solution for which, $k = k^{max}$ at $-\Delta G^{o\prime} = \lambda$ and is a consequence of the contribution from multiple levels in the oxide below the Fermi level. The inset in Figure 3 shows the ratio $k_{1/2}/k_{1/2}{}^{max}$ plotted against both E_{app} and $\Delta G^{o\prime}{}_{bet}$ illustrating experimental verification of this prediction. The line overlaying the data was calculated from the ratio $k_{1/2}/k_{1/2}{}^{max}$ and eq 7 with $\lambda = 0.56$ eV. The condition, $-\Delta G^{o\prime}{}_{bet} = \lambda$, with $k_{1/2}/k_{1/2}{}^{max} = 0.5$ is indicated in the inset.

According to eq 6, the maximum rate constants for back electron transfer should be proportional to both N and H_{ab}. The experimental ratio $k_{1/2}{}^{max}(red)/k_{1/2}{}^{max}(ox) = 1.7$ is nearly equal to the ratio of electron densities, $N(red)/N(ox) = 2.5$, obtained by analysis of the near-IR LSPR feature mentioned above consistent with back electron transfer proportional to the electron density of the oxide. In terms of H_{ab}, it is notable that experimental values for the maximum rate constants for back electron transfer, $k_{1/2}{}^{max} = 2.3$ and $4.0 \times 10^8\ s^{-1}$, are relatively small and point to relatively weak electronic coupling to the nanoITO surface.

The photoinduced electron-transfer behavior observed for the nanoITO−RuP^{2+} electrodes is summarized in the Gerischer diagram in Scheme 1. It assumes a constant $g(E)$ for nanoITO with electron occupancy defined in the low-temperature limit such that filled levels exist at $E > E_F$ and unfilled levels at $E < E_F$. Although not explored in detail here, electron injection (k_{inj}) from the thermally equilibrated excited-state $-RuP^{2+*}$, is illustrated and depends on the overlap of unfilled levels in nanoITO with the excited-state distribution function $W_{Ru2+*}(E)$, defined by the reorganizational energy λ^* (purple dashed region).

As shown in the diagram and demonstrated here, back electron transfer (k_{bet}) depends on the overlap of filled levels in nanoITO

dx.doi.org/10.1021/ja508862h | J. Am. Chem. Soc. 2014, 136, 15869−15872

Scheme 1. Gerischer Diagram Depicting the Energetics Associated with Electron Injection by $-RuP^{2+*}$ and Back Electron Transfer to $-RuP^{3+}$ (see text for further description)

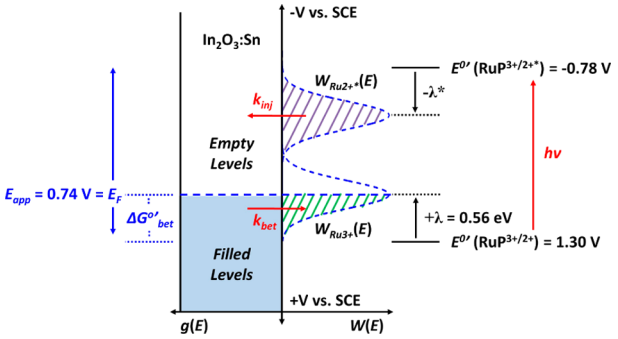

with the ground-state distribution function $W_{Ru3+}(E)$, defined by the reorganization energy λ (green dashed region). The special condition, $-\Delta G^{o\prime}{}_{bet} = \lambda$, is shown in the scheme at $E_{app} = E_F$ = 0.74 V vs SCE where half of the $W_{Ru3+}(E)$ Gaussian distribution function is overlapped with filled levels in the oxide leading to $k_{bet} = k_{bet}{}^{max}/2$, as discussed above.

The results reported here are important in demonstrating, for the first time, the use of a derivatized nanoTCO film to explore the role of driving force in interfacial, molecular electron-transfer kinetics over a range of nearly 2 eV. The ability to use an applied external bias to control driving force over a wide potential range is in contrast to intrinsic semiconductor nanoparticle films of the oxides TiO_2, SnO_2, and ZnO. For those oxides the range of applied biases is limited to the conduction band edge and above. The kinetic facility, optical transparency, and high density of electrons in nanoITO enable kinetic parameters to be obtained for single redox sites in contrast to solution measurements where two redox sites are required. The driving force dependence on the rate constant for back electron transfer was found to be consistent with Marcus–Gerischer theory with an average reorganization energy of $\lambda = 0.56 \pm 0.04$ eV for the $Ru^{III/II}$ couple, comparable to values obtained from solution measurements for $[Ru(bpy)_3]^{3+/2+}$ self-exchange. Finally, the experimental protocols and analyses reported here are general, and we anticipate that the procedures described will find broad usage in characterizing interfacial electron-transfer reactions for a wide range of surface-bound molecules.

■ ASSOCIATED CONTENT

Supporting Information

Experimental details and additional figures. This material is available free of charge via the Internet at http://pubs.acs.org.

■ AUTHOR INFORMATION

Corresponding Author

tjmeyer@unc.edu

Notes

The authors declare no competing financial interest.

■ ACKNOWLEDGMENTS

This material is based upon work supported by the U.S. Department of Energy, Office of Science, Office of Basic Energy Sciences, under award no. DE-FG02-06ER15788.

■ REFERENCES

(1) Ardo, S.; Meyer, G. J. *Chem. Soc. Rev.* **2009**, *38*, 115.
(2) Gratzel, M. *Nature* **2001**, *414*, 338.
(3) Hagfeldt, A.; Boschloo, G.; Sun, L.; Kloo, L.; Pettersson, H. *Chem. Rev.* **2010**, *110*, 6595.
(4) Anderson, N. A.; Lian, T. *Annu. Rev. Phys. Chem.* **2005**, *56*, 491.
(5) Benkö, G.; Kallioinen, J.; Korppi-Tommola, J. E. I.; Yartsev, A. P.; Sundström, V. *J. Am. Chem. Soc.* **2002**, *124*, 489.
(6) Katoh, R.; Furube, A.; Barzykin, A. V.; Arakawa, H.; Tachiya, M. *Coord. Chem. Rev.* **2004**, *248*, 1195.
(7) Tachibana, Y.; Haque, S. A.; Mercer, I. P.; Moser, J. E.; Klug, D. R.; Durrant, J. R. *J. Phys. Chem. B* **2001**, *105*, 7424.
(8) Barzykin, A. V.; Tachiya, M. *J. Phys. Chem. B* **2002**, *106*, 4356.
(9) Nelson, J.; Haque, S.; Klug, D.; Durrant, J. *Phys. Rev. B* **2001**, *63*, 205321.
(10) Haque, S. A.; Tachibana, Y.; Klug, D. R.; Durrant, J. R. *J. Phys. Chem. B* **1998**, *102*, 1745.
(11) Bisquert, J. *J. Phys. Chem. C* **2007**, *111*, 17163.
(12) Youngblood, W. J.; Lee, S. A.; Kobayashi, Y.; Hernandez-pagan, E. A.; Hoertz, P. G.; Moore, T. A.; Moore, A. L.; Gust, D.; Mallouk, T. E. *J. Am. Chem. Soc.* **2009**, *131*, 926.
(13) Song, W.; Vannucci, A. K.; Farnum, B. H.; Lapides, A. M.; Brennaman, M. K.; Kalanyan, B.; Alibabaei, L.; Concepcion, J. J.; Losego, M. D.; Parsons, G. N.; Meyer, T. J. *J. Am. Chem. Soc.* **2014**, *136*, 9773.
(14) Gao, Y.; Ding, X.; Liu, J.; Wang, L.; Lu, Z.; Li, L.; Sun, L. *J. Am. Chem. Soc.* **2013**, *135*, 4219.
(15) Alibabaei, L.; Brennaman, M. K.; Norris, M. R.; Kalanyan, B.; Song, W.; Losego, M. D.; Concepcion, J. J.; Binstead, R. A.; Parsons, G. N.; Meyer, T. J. *Proc. Natl. Acad. Sci. U. S. A.* **2013**, *110*, 20008.
(16) Gerischer, H. *Photochem. Photobiol.* **1972**, *16*, 243.
(17) Gerischer, H.; Willig, F. *Top. Curr. Chem.* **1976**, *61*, 31.
(18) Marcus, R. A. *Annu. Rev. Phys. Chem.* **1964**, *15*, 155.
(19) Royea, W. J.; Fajardo, A. M.; Lewis, N. S. *J. Phys. Chem. B* **1997**, *101*, 11152.
(20) Clifford, J. N.; Palomares, E.; Nazeeruddin, K. M.; Gratzel, M.; Nelson, J.; Li, X.; Long, N. J.; Durrant, J. R. *J. Am. Chem. Soc.* **2004**, *126*, 5225.
(21) Moser, J. E.; Gratzel, M. *Chem. Phys.* **1993**, *176*, 493.
(22) Kuciauskas, D.; Freund, M. S.; Gray, H. B.; Winkler, J. R.; Lewis, N. S. *J. Phys. Chem. B* **2001**, *105*, 392.
(23) Nelson, J.; Chandler, R. E. *Coord. Chem. Rev.* **2004**, *248*, 1181.
(24) Nelson, J. *Phys. Rev. B* **1999**, *59*, 374.
(25) Albery, W. J.; Bartlett, P. N. *J. Electrochem. Soc.* **1984**, *131*, 315.
(26) Boschloo, G.; Fitzmaurice, D. *J. Phys. Chem. B* **1999**, *103*, 3093.
(27) Zum Felde, U.; Haase, M.; Weller, H. *J. Phys. Chem. B* **2000**, *104*, 9388.
(28) Farnum, B. H.; Morseth, Z. A.; Lapides, A. M.; Rieth, A. J.; Hoertz, P. G.; Brennaman, M. K.; Papanikolas, J. M.; Meyer, T. J. *J. Am. Chem. Soc.* **2014**, *136*, 2208.
(29) Garcia, G.; Buonsanti, R.; Runnerstrom, E. L.; Mendelsberg, R. J.; Llordes, A.; Anders, A.; Richardson, T. J.; Milliron, D. J. *Nano Lett.* **2011**, *11*, 4415.
(30) Llordés, A.; Garcia, G.; Gazquez, J.; Milliron, D. J. *Nature* **2013**, *500*, 323.
(31) Lounis, S. D.; Runnerstrom, E. L.; Bergerud, A.; Nordlund, D.; Milliron, D. J. *J. Am. Chem. Soc.* **2014**, *136*, 7110.
(32) Mendelsberg, R. J.; Garcia, G.; Li, H.; Manna, L.; Milliron, D. J. *J. Phys. Chem. C* **2012**, *116*, 1226.
(33) Nütz, T.; zum Felde, U.; Haase, M. *J. Chem. Phys.* **1999**, *110*, 12142.
(34) Hamberg, I.; Granqvist, C. G. *J. Appl. Phys.* **1986**, *60*, R123.
(35) Hanson, K.; Brennaman, M. K.; Ito, A.; Luo, H.; Song, W.; Parker, K. A.; Ghosh, R.; Norris, M. R.; Glasson, C. R. K.; Concepcion, J. J.; Lopez, R.; Meyer, T. J. *J. Phys. Chem. C* **2012**, *116*, 14837.
(36) Hoertz, P. G.; Chen, Z.; Kent, C. A.; Meyer, T. J. *Inorg. Chem.* **2010**, *49*, 8179.
(37) Young, R. C.; Keene, F. R.; Meyer, T. J. *J. Am. Chem. Soc.* **1977**, *99*, 2468.
(38) Sutin, N. *Acc. Chem. Res.* **1982**, *15*, 275.